

Image Denoising Using Anisotropic Second and Fourth Order Diffusions Based on Gradient Vector Convolution

Huaibin Wang, Yuanquan Wang^{*}, and Wenqi Ren

School of Computer and Communication engineering, Tianjin University of
Technology, 300384 Tianjin, China

^{*}Corresponding Author: yqwang@bit.edu.cn

Abstract. In this paper, novel second order and fourth order diffusion models are proposed for image denoising. Both models are based on the gradient vector convolution (GVC) model. The second model is coined by incorporating the GVC model into the anisotropic diffusion model and the fourth order one is by introducing the GVC to the You-Kaveh fourth order model. Since the GVC model can be implemented in real time using the FFT and possesses high robustness to noise, both proposed models have many advantages over traditional ones, such as low computational cost, high numerical stability and remarkable denoising effect. Moreover, the proposed fourth order model is an anisotropic filter, so it can obviously improve the ability of edge and texture preserving except for further improvement of denoising. Some experiments are presented to demonstrate the effectiveness of the proposed models.

Keywords: Gradient vector convolution, fourth order diffusion, anisotropic diffusion, noise removal, texture preserving.

1. Introduction

Image denoising is one of the fundamental topics of research in image processing and computer vision, whose main goal is to eliminate the noise and preserve edges in image. During the last two decades, partial differential equations (PDEs) have been justified as effective tools for image smoothing, which are able to achieve a good trade-off between noise removal and edge-preserving. Cacelles et al. generally explained the superiority of PDEs-based denoising in [1]. Besides PDE-based methods, some recently developed non-diffusion based approaches can also bring considerable improvement in denoising performance, such as the kernel regression (LARK) [2], bilateral filter [3], patch-based methods [4-5], wavelet-based methods [6-7] and the BM3D based on sparse representation [8]. In this paper, we will focus on the PDE-based diffusion methods.

The anisotropic diffusion introduced by Perona and Malik (P-M) [9] can be considered as a typical feature-preserving denoising algorithm, where diffusion is controlled by a variable coefficient in order to preserve edges. Since the

work of Perona and Malik [9], there have been extensive literatures that present a variety of PDEs-based anisotropic diffusion models and offer diverse numerical schemes to obtain the steady-state solution [10]-[18], [31-32]. Details of the behavioral of the anisotropic diffusion can be found in [10]. Scherzer et al. [11] investigated connections between regularization theory and framework of diffusion filtering. Catte et al. [12-13] proved the ill-posedness of the P-M equation and proposed a modified diffusion coefficient which is a function of a smoothed gradient. Rudin et al. introduced Shock filters [14] and total variation [15] minimization. The works in [14] opened the possibility to reformulate the image enhancement as a combination of two coupled terms that implement inverse and forward diffusion processes. Alvarez and Mazorra [16] combined the shock filter and a diffusion term for image enhancement. Gilboa et al. [17] proposed a forward and backward (FAB) adaptive diffusion process that enhances features while locally denoising smoother segments; later, they introduced the complex diffusion for ramp-preserving [18]. Black et al. [19] illustrated the relations between anisotropic diffusion and robust statistics. In [20], a method was proposed for texture preserving by adding a spatially varying fidelity term. Another interesting work [21] was the incorporation of the gradient vector flow (GVF) field [22], which is originally introduced as an external force for active contour model [23], into the anisotropic diffusion. Ghita et al. [24] introduced a new modified GVF (INGVF) field into the P-M equation in order to improve the denoising effect. Sum et al. [25] proposed a stabilization method to make the GVF-based P-M equation stable. The proposed GVF-based P-M equation can improve the denoising effect, but the computational cost is expensive.

Although the second-order anisotropic diffusion is effective for image noise removal, it can lead to staircase effect. These staircases are visually unpleasant and can be falsely detected as edges. In order to alleviate this staircase effects, a number of authors have proposed high order PDEs for image denoising [26-28], [33-34]. One of the most popular fourth-order PDEs is introduced by You-Kaveh (Y-K) [27], which seeks to approximate the noisy image with a piecewise harmonic one. Another classical fourth-order model was proposed by Lasaker, Lundervold and Tai (LLT) [28], in which two different functions have been proposed to measure the oscillations in the noisy data. The fourth-order filters damp high frequency components of images much faster than the second-order peers, this means the fourth-order models would over-smooth the step edges in images. In addition, they can also cause speckle noise in the filtered image.

In this paper, we first introduce the gradient vector convolution (GVC) model [29] into the anisotropic P-M equation. The GVC model is our previous work, which serves as external force for active contours. It is very robust to noise and can be calculated in real time. The new GVC-based P-M equation has many desirable properties, such as superior noise robustness, reduced computational cost, and the improved denoising effect. Second, the GVC field is introduced into Y-K model; the proposed GVC-based fourth order model is anisotropic because the diffusions along the directions of level set and gradient are uneven. Thus, the modified Y-K model could not only improve

peak-signal-to-noise ratio (PSNR) of the filtered image, but also keep edge and texture information in the filtered image.

This paper is organized as follows: Section 2 briefly introduces the second order and fourth order approaches for image denoising. Section 3 details the proposed method of GVC-based second order and fourth order models. The experimental results are provided in Section 4. Finally, the conclusion is given in Section 5.

2. Related Works

2.1. Second Order diffusion: P-M Model and INGVF-based P-M Model

The anisotropic diffusion proposed by Perona and Malik [9] takes the following form

$$\begin{cases} \partial u / \partial t = \operatorname{div}(c(|\nabla u|)\nabla u) \\ u(x, y, t = 0) = u_0(x, y) \end{cases} \quad (1)$$

where ∇ is the gradient operator, div is the divergence operator and $c(\cdot)$ is the diffusion coefficient. The diffusion coefficient is a positive and non-increasing function over $|\nabla u|$. The coefficient plays an important role in diffusion and it usually takes one of the following two forms:

$$c(|\nabla u|) = \frac{1}{1 + (|\nabla u|/k)^2} \quad (2)$$

$$c(|\nabla u|) = \exp\left(-(|\nabla u|/k)^2\right) \quad (3)$$

where k is so-called contrast parameter. When k is a small value, weak edges will be preserved while the denoising capability is weak. When k is a large value, the denoising capability is strong, but weak edges and fine details will be smoothed as well.

Equation (1) was associated with the following energy function [10]

$$E(u) = \int_{\Omega} f(|\nabla u|) d\Omega \quad (4)$$

where Ω is image domain, and $f(\cdot)$ is an increasing function over $|\nabla u|$.

The key idea of P-M equation is to roughly smooth out the homogeneous regions when $|\nabla u|$ is small and to enhance the boundaries instead when $|\nabla u|$ is large.

So far, much research has been devoted to improving the P-M anisotropic

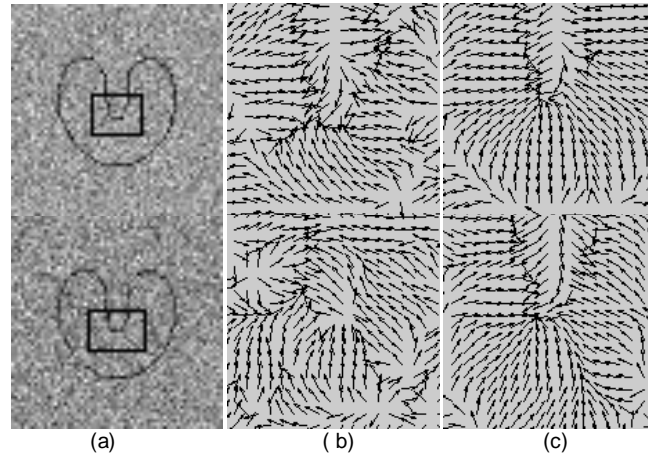


Fig.1. (a) noisy u-shape image corrupted with Gaussian noise $N(0,0.3)$ in first row and $N(0,0.4)$ in second row; (b) GVF field; (c) GVC field with $n=2, h=10$. The computing time for GVF and GVC are 0.45s and 0.048s, respectively.

diffusion method. One of the most important directions is Yu-Chua's work [21]. Although the P-M equation forms a solid foundation for other research of anisotropic diffusion models, its numerical stability still needs to be improved. Building on this concept, Yu and Chua introduced the GVF field in P-M model as follows

$$\frac{\partial u}{\partial t} = -\mathbf{V}_{GVF} \cdot \nabla u + c(|\nabla u|)\nabla^2 u \quad (5)$$

where ∇^2 is the Laplacian operator, \mathbf{V}_{GVF} is the GVF field which is proposed in [22]. The GVF-based P-M equation shows an improved performance of numerical stability when compared to original P-M equation. However, it is important to note that the (5) needs long computing time as the GVF field is calculated by iteratively solving diffusion PDEs on the whole image. Another similar method is proposed by Ghita and Whelan in [24]. In this paper, they proposed a new GVF (INGVF) which shows a better performance in the presence of impulse noise. Then, they combined the modified P-M model with adaptive median filter and gave the INGVF-based P-M model

$$\frac{\partial u}{\partial t} = (1 - IN_{Est}(u)) \left(med(u) - \frac{\partial u}{\partial (t-1)} \right) + IN_{Est}(u) \left[-\mathbf{V}_{INGVF} \cdot \nabla u + c \cdot \nabla^2 u \right] \quad (6)$$

where med denotes the adaptive median filter, IN_{Est} is the impulse estimator defined in [24] and \mathbf{V}_{INGVF} is the INGVF. The key idea of INGVF-based P-M equation is to smooth image by the first term in (6) when the image is

Image Denoising Using Anisotropic Second and Fourth Order Diffusions Based on Gradient Vector Convolution

corrupted by impulse noise and smooth image by the second term in (6) when

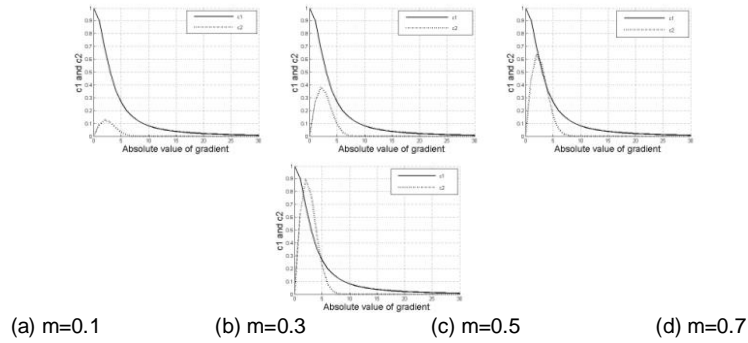


Fig.2. Diffusion functions of c_1 and c_2 with parameter m change ($k_1 = k_2 = 3$).

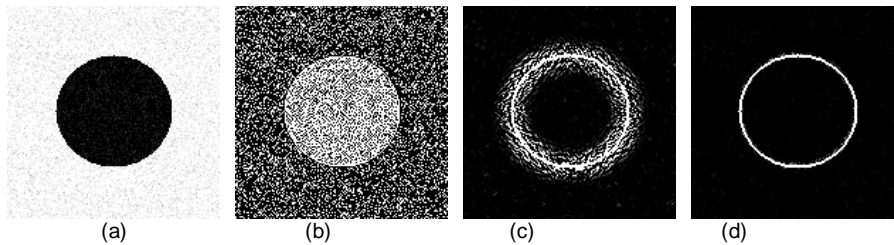


Fig.3. (a) noisy image corrupted by Gaussian noise— $N(0,20)$; (b) $u_{\eta\eta}$ calculated directly; (c) GVF-based $u_{\eta\eta}$; (d) GVC-based $u_{\eta\eta}$.

the image is corrupted by Gaussian noise. We could see that the intrinsic nature of impulse noise removal is through the median filter and the filter of Gaussian noise removal corresponding to (6) is as follow

$$\frac{\partial u}{\partial t} = -\mathbf{V}_{IN_{GVF}} \cdot \nabla u + c(|\nabla u|) \nabla^2 u \quad (7)$$

In (7), INGVF field even need a longer computing time than the GVF because it need to calculate the impulse estimator IN_{Est} besides the iteratively solving diffusion PDEs on the whole image.

2.2. Fourth Order Diffusion: Y-K model

Although the anisotropic diffusion is an effective method for image noise removal, it tends to cause staircase effect. In order to resolve this problem, You and Kaveh [27] introduced a fourth-order PDE-based denoising method in which the filtered image is obtained by minimizing the following functional

$$E(u) = \int_{\Omega} f(|\nabla^2 u|) d\Omega \quad (8)$$

where $|\nabla^2 u|$ is simply an absolute value of Laplacian of u approximated by $|u_{xx} + u_{yy}|$. By using calculus of variation, the Euler equation to minimize (8) reads

$$\frac{\partial u}{\partial t} = -\nabla^2 \left(c(|\nabla^2 u|) \nabla^2 u \right) \quad (9)$$

This fourth-order PDE favors a piecewise harmonic image, i.e., $\nabla^2 u \rightarrow 0$ locally, as $t \rightarrow \infty$. It is believed the piecewise harmonic image is a better approximate than the piecewise constant one to a natural image, and numerical results presented in [27] verified that the staircase effect is reduced and the image looks more natural.

3. GVC-based Second and Fourth Order Diffusions

3.1. GVC: Gradient Vector Convolution [29]

Gradient vector convolution (GVC) field was presented as an external force for active contour. The GVC field is motivated by gradient vector flow (GVF) field and possesses all advantages of GVF, such as enlarged capture range, initialization insensitivity and high performance on concavity convergence. However, the GVC can outperform GVF in term of computational time because the GVF is constructed by iteratively solving diffusion PDEs on the whole image while the GVC is implemented by convolving the gradient vector with a certain kernel. The GVC field $V=(u(x,y), v(x,y))$ is the solution of the following equation

$$\begin{cases} u(x, y) = f_x(x, y) * K(x, y) \\ v(x, y) = f_y(x, y) * K(x, y) \end{cases} \quad (10)$$

where $*$ denotes convolution operation, $f(x,y)$ is the edge map of an image, (f_x, f_y) is the gradient vector of image edge map, $K(x,y)$ is the convolution kernel and in practice $K(x, y) = 1/r_h^n$, $h, n \in R^+$, $r_h = \sqrt{x^2 + y^2 + h}$. The factor h plays a role analogous to scale space filtering. The GVC field has superior robustness on Gaussian noisy images. In addition, it can be implemented in real time owing to its convolution mechanism. Fig. 1 illustrates the excellent performance of GVC fields on a noisy image comparing with the GVF field. In this section, the GVF field parameters are $\mu = 0.2$, and 80 iterations, the GVC field parameters are $n=2$, $h=10$, the kernel size is the same as that of the image (image size is 64×64).

3.2. GVC-Based P-M Model

In this section, we introduce the GVC-based P-M model for image denoising.

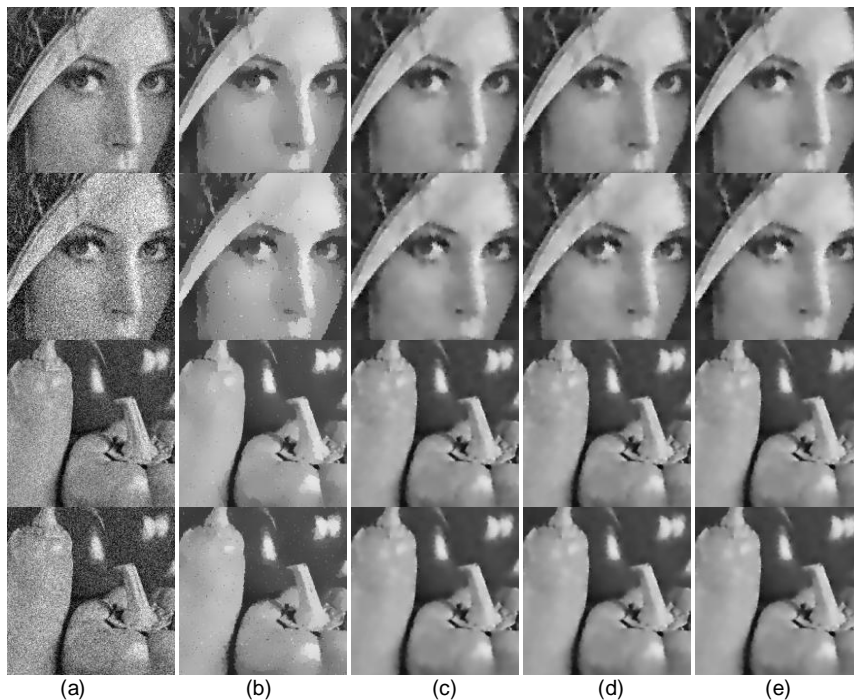


Fig.4. (a) Noisy images, results by (b) P-M equation, (c) GVF-based P-M equation, (d) INGVF-based P-M equation, (e) GVC-based P-M equation. The noise variance is 20 in the first and third rows and 30 the second and fourth rows, respectively.

Here we shall briefly mention that the two advantages of the proposed GVC-based P-M model: 1) it can improve the denoising effect; and 2) the computing time is reduced due to convolution mechanism of GVC.

As shown in Fig.1, the GVC can be implemented in real time and is more robust to noise when compared with the GVF model. As a result, it is natural to introduce the GVC into the P-M models to propose an improvement of the GVF-based anisotropic diffusion [21] and the INGVF-based one [24]. The P-M model is first expanded as

$$\frac{\partial u}{\partial t} = c(|\nabla u|)\nabla^2 u + c'\nabla|\nabla u|\cdot\nabla u \quad (11)$$

It has been pointed out in [21] that the second term is an inverse diffusion term for sharpening the boundaries while the first term is a Laplacian term for smoothing the regions that are relatively flat. Using the term $-\mathbf{V}\cdot\nabla u$ to approximate the inverse diffusion term in Eq.(11), we get the GVC-based diffusion as follows,

$$\frac{\partial u}{\partial t} = -\mathbf{V} \cdot \nabla u + c(|\nabla u|)\nabla^2 u \tag{12}$$

where \mathbf{V} denotes the GVC field. In (12), \mathbf{V} have been determined before image evolution, only ∇u needs to be computed directly from the observed images in the inverse diffusion term. The proposed model possesses all advantages of GVF-based P-M equation, such as robust estimation of the high-order derivative and improvement of numerical stability. Moreover, the GVC-based diffusion will benefit from the computational cost and noise robustness of the GVC model.

Table 1. Quantitative Comparison of the Results of Fig.4

Image(σ)	Method	PSNR	MSSIM	Iterations	Time(s) of GVF/INGVF/GVC	
Lena	20	P-M model [9]	29.28	0.78	175	
		GVF-based [21]	29.61	0.81	25	35.81
		INGVF-based [24]	29.61	0.81	25	56.49
		GVC-based(12)	30.18	0.82	25	1.96
	30	P-M model [9]	27.06	0.71	380	
		GVF-based [21]	28.33	0.78	45	35.81
		INGVF-based [24]	28.33	0.78	45	56.49
		GVC-based(12)	28.98	0.80	45	1.96
Pepper	20	P-M model [9]	29.44	0.70	175	
		GVF-based [21]	29.84	0.76	20	35.81
		INGVF-based [24]	29.84	0.76	20	56.49
		GVC-based(12)	29.90	0.78	20	1.96
	30	P-M model [9]	27.05	0.62	370	
		GVF-based [21]	27.74	0.73	40	35.81
		INGVF-based [24]	27.74	0.73	40	56.49
		GVC-based(12)	27.81	0.75	40	1.96

3.3. GVC-Based Y-K Model

The Y-K model can alleviate effectively the staircase effect, but it is isotropic and performs poor on preserving edge and texture. In this section we introduce the GVC field in the Y-K model so that it becomes an anisotropic diffusion model. To this purpose, we modify the Y-K equation as

$$\frac{\partial u}{\partial t} = -\nabla^2 (c_1 \Delta u - c_2 u_{\eta\eta}) \tag{13}$$

where η is the direction of gradient, c_1 and c_2 are the diffusion coefficients.

3.3.1. The Choice of Diffusion Coefficients

Some important analysis about the diffusion coefficients need to be highlighted. Obviously, if $c_2 = 0$, Eq.(13) becomes the isotropic one (9). If $c_1 < c_2$, the overall diffusion on the gradient direction will become backward, which damages the image feature. If $c_1 = c_2$, the diffusion on the gradient direction will disappear both in intra-region and in inter-region. In light of the above analysis, we make $c_1 > c_2$ so that the overall diffusion along the gradient direction is smaller than the one along the direction of level set.

In addition to let $c_1 > c_2$, we need to make the coefficient function c_2 close to zero for $|\nabla u| \rightarrow 0$, while c_2 close to c_1 for $|\nabla u| \rightarrow \infty$. So that the diffusion on the direction of the gradient is large in intra-region and it is small in inter-region. Equation (3) multiplied with $|\nabla u|$ can meet the above demand. So in our implementation, the diffusion functions c_1 and c_2 take the following forms

$$c_1(|\nabla u|) = \frac{1}{1 + (|\nabla u|/k_1)^2} \quad (14)$$

$$c_2(|\nabla u|) = m \cdot |\nabla u| \cdot \exp\left(-(|\nabla u|/k_2)^2\right), 0 < m \leq 1 \quad (15)$$

One can adapt the parameters k_1 , k_2 and m according to the smoothing effect. When parameter m increasing, the value of c_2 will be larger than c_1 in some region as in Fig.2, which damages the image feature. Therefore, we need set a suitable value for m so that $c_2 < c_1$ in the entire image region. In this paper, we make $m = 0.3$. This is illustrated in Fig.2.

3.3.2. The Substitute of Second-order Derivative $u_{\eta\eta}$

It is important to note that the second-order derivative $u_{\eta\eta}$ in (13) is computed from the image at each iteration. Since high-order derivative is sensitive to noise, the numerical stability of $u_{\eta\eta}$ will be reduced owing to the influence of the noise. In this paper we will replace $u_{\eta\eta}$ with $\mathbf{V}_{GVC} \cdot \mathbf{N}$, $\mathbf{N} = \nabla u / |\nabla u|$. We illustrate the improved performance of substitution of $\mathbf{V}_{GVC} \cdot \mathbf{N}$ for $u_{\eta\eta}$ and $\mathbf{V}_{GVF} \cdot \mathbf{N}$ on a synthetic image in Fig. 3. In this section the GVF field is calculated with $\mu = 0.2$ with 80 iterations and the GVC field parameters are $n=3$, $h=20$, the kernel size is 32×32 (image size 128×128). As can be seen from Figs. 3 (b)-(d), $u_{\eta\eta}$ and GVF-based $u_{\eta\eta}$ are seriously

affected by noise while the GVC-based $u_{\eta\eta}$ is near perfect and most of noise points are effectively overcome. As $\mathbf{V}_{GVC} \cdot \mathbf{N}$ can effectively approximate the second derivative $u_{\eta\eta}$, the scheme of (13) can be rewritten as

$$\frac{\partial u}{\partial t} = -\Delta(c_1 \Delta u - c_2 \mathbf{V}_{GVC} \cdot \mathbf{N}) \quad (16)$$

Since the GVC field has been determined before image evolution, only first derivative needs to be computed directly from the being filtered images. The proposed method not only possesses anisotropic characteristics, but also improves the numerical stability.

4. Experimental Results

We conduct several experiments to demonstrate the properties of the proposed methods. First, the proposed GVC-based P-M model is compared with the P-M [9], GVF-based P-M [21] and INGVF-based P-M [24] models. Then, the denoising effect and the ability of edge and texture preserving of the GVC-based Y-K model are evaluated on several real images. In order to evaluate the quality of the filtered images, the peak-signal-to-noise ratio (PSNR) and mean structure similarity (MSSIM) [30] are employed as objective indices.

4.1. Experimental Results: GVC-Based P-M Model

In order to demonstrate the desirable properties of the proposed second order model, the Lena and Pepper images are employed as test images, the dimension of both images are 512×512 . Noisy images are coined by adding zero-mean Gaussian noise of various standard deviations. The time step for all the second-order models is 0.2, and the diffusion function $c(|\nabla u|)$ takes the form in Eq.(2) with $k = 3$. The factor μ is 0.2 and the iteration number is 100 in all GVF field. The GVC field parameters are as follows: $h = 10$ and $n = 2$, the kernel size is 64×64 . Fig.4 shows the results. It is clear that the GVF, INGVF and GVC-based models successfully avoid the staircases and yield visually pleasant results. Although the results by the GVF, INGVF and GVC-based models are visually comparable, the PSNR and MSSIM indices in Table 1 manifest that the GVC-based model outperforms the other models. In this Figure, only a part of the images are shown for the sake of clarity.

4.2. Experimental Results: GVC-Based Y-K Model

4.2.1. Test of Denoising

In order to demonstrate the desirable properties of the proposed model in Eq.(16), we first use the *Lena* (512×512) image corrupted with different noise level to examine the performance of the proposed fourth order filter. The *Lena* image is corrupted by zero-mean Gaussian noise of deviation 15 and 30. In addition to the classical fourth order diffusion method Y-K model [27] and LLT model [28], the results are also compared with that of the non-local mean



Fig.5. (a) original *Lena* image; (b) noisy image: $N(0,15)$; (c) Y-K [27], Time=152.04(s); (d) LLT [28], Time=10.20(s); (e) non-local mean [4]; (f) LARK [2], Time=570.09(s); (g) BM3D [8], Time=6.99(s); (h) proposed GVC-based Y-K, Time=120.27(s).

(NLM) [4], LARK [2], and BM3D [8]. In all the following experiments, the

parameters of the proposed model are: $m=0.3$, $k_1=k_2=3$, $\Delta t=0.03$, and $h=10$, $n=2$ for GVC and the kernel size is a quarter of the size of the test images. The time step for Y-K and LLT models is $\Delta t=0.2$. The results of the NLM are yield from the IPOL¹ website, so the parameters for the NLM are



Fig.6. (a) original Lena image; (b) noisy image: $N(0,30)$; (c) Y-K [27], Time=654.21(s); (d) LLT [28], Time=26.73(s); (e) non-local mean [4]; (f) LARK [2], Time=1419.20(s); (g) BM3D[8], Time=7.04s; (h) proposed GVC-based Y-K, Time=450.28s.

default. We adopt the software packages of the LARK² and BM3D³ and the parameters for both models are unchanged as in the package. In addition to the PSNR, we also compared the computing time of these models except NLM method because the results of the NLM are yield from website and we cannot get an accurate computational time. The visual results of applying different

¹ http://www.ipol.im/pub/algo/bcm_non_local_means_denoising/

² <http://users.soe.ucsc.edu/~milanfar/software/>

³ http://www.cs.tut.fi/~foi/GCF-BM3D/index.html#ref_papers

enhancement techniques on the Lena image with different noise levels are shown in Figs.5-6. One can visualize from the Figs.5-6 that the proposed method performs better in terms of denoising effect than the other fourth order models and NLM method, though less effect than the LARK and BM3D models. Besides, the computing time of GVC-based YK model is shorter than the Y-K and LARK model. This set of experiments show that the GVC-based Y-K model performs better than Y-K, LLT and NLM models for denoising effect and shorter than Y-K and LARK models for computing time. The BM3D is the best model not only in denosing effect but also in computing time. However, we focus on diffusion-based methods in this paper, so we only compare the diffusion-based models in the following experiments.

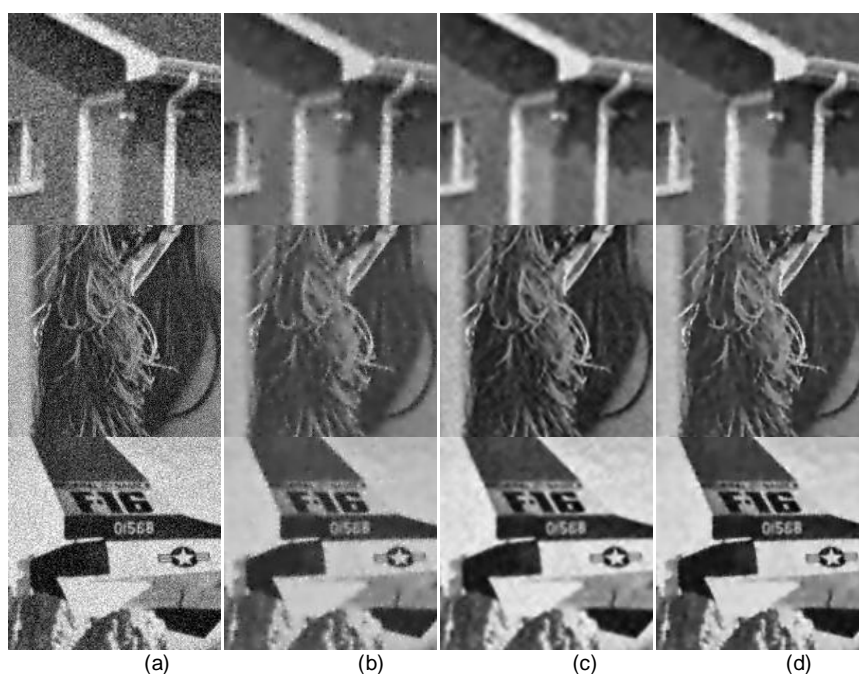


Fig.7. (a) noisy images with zero-mean Gaussian noise of deviation 20, results by (c) Y-K model[20], (d) LLT model[21], and (e) proposed fourth order model. The House, Lena and airplane images are shown in from the first to the third rows, respectively, only a part of the images are shown for the sake of clarity.

The previous two experiments are conducted for various noise levels. The next set of experiments is conducted for different images with same noise level. The *House* (256×256), *Lena* (512×512) and *Airplane* (512×512) images are employed as test images. As we can see in Figs.5-6, the methods of LARK and BM3D perform better than the diffusion model. So the results in this experiment are compared only with that of the diffusion method: Y-K model [27] and LLT model [28]. The three images are corrupted by zero-mean Gaussian noise of deviation 20. The algorithms terminated when the PSNR of

the filtered images reaches maximum.

Table 2. Quantitative Comparison of the Results of Fig.7

Image	Method	PSNR(dB)	MSSIM	Iterations
House	Y-K [27]	28.83	0.76	588
	LLT [28]	29.37	0.78	51
	GVC-based(16)	30.46	0.82	246
Lena	Y-K [27]	29.92	0.81	676
	LLT [28]	30.95	0.82	67
	GVC-based(16)	31.15	0.84	280
Airplane	Y-K [27]	28.85	0.81	567
	LLT [28]	29.71	0.82	51
	GVC-based(16)	30.94	0.87	279

The PSNR and MSSIM indices are also employed as objective index to evaluate the quality of the filtered images. Fig.7 shows the results, only a part of the images are shown for the sake of clarity. It is clear that the Y-K model suffers from speckle noise and the LLT and proposed models avoid the speckle noise successfully. Meanwhile, the Y-K and LLT models over-smooth the edges and the proposed model preserves edges much better, see the digital number '568' in the airplane image. The PSNR and MSSIM indices shown in Table 2 also manifest the high performance of the proposed model.

4.2.2. Test of Edge and Texture Preserving

In the following experiments, we illustrate the performance of the proposed model on preserving edge and texture. To evaluate the quality of the denoised image, we employ the intensity residual which is given by

$$u_{residual} = u_{denoised} - u_{noise} \quad (17)$$

where $u_{denoised}$ denotes the denoised images and u_{noise} denotes noisy image. If there is less texture information in residual, this method is considered to be better. We use two images with large amount of texture information: Barbara and Room as test images.

Figs.8-9 show the experimental results on Barbara and Room, respectively. From the intensity profiles of the selected lines, see Figs.8-9 (e), it is clear that the results by the proposed model are smoother and preserves the step edges better than the Y-K model and LLT model. From the intensity residuals, see Figs.8-9 (f)-(h), one can conclude that the proposed model largely reduced the texture information in the residuals, which means the proposed model can preserve texture much better than the Y-K model and LLT model. The experimental results indicate that the GVC-based fourth order model shows an improved performance on preserving edge and texture compared with the original Y-K model and LLT model.

Image Denoising Using Anisotropic Second and Fourth Order Diffusions Based on Gradient Vector Convolution

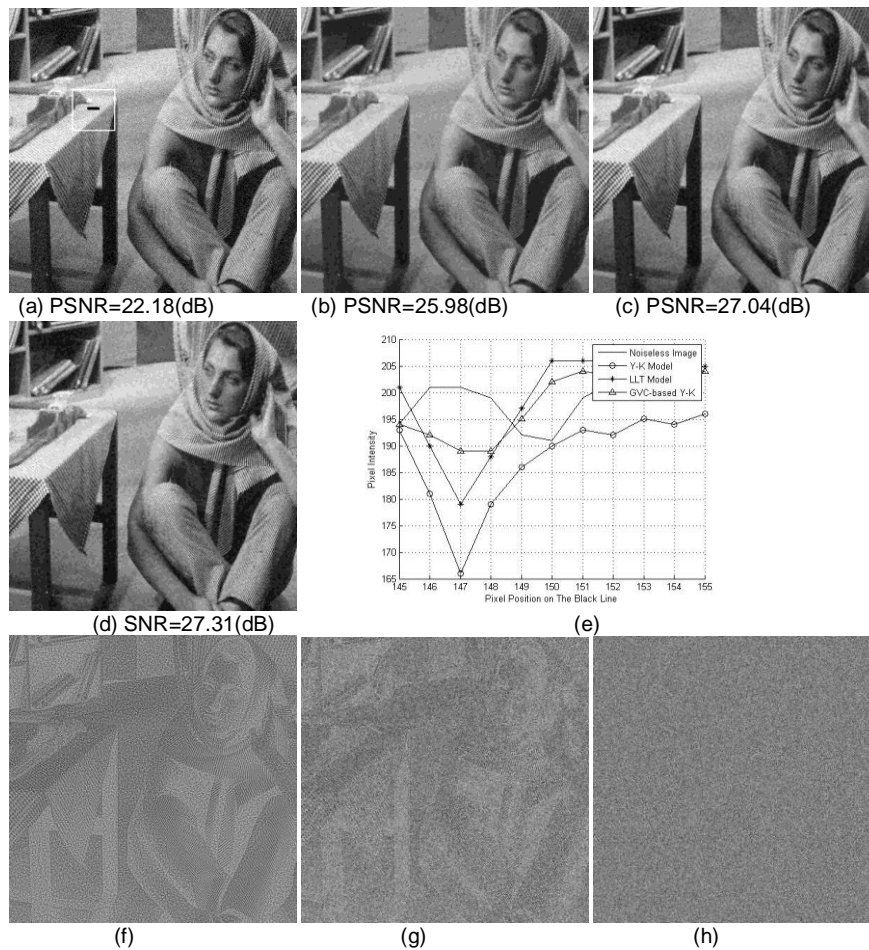


Fig.8. (a) Barbara image corrupted with Gaussian noise— $\mathcal{N}(0,20)$; (b) Y-K model; (c) LLT model; (d) GVC-based Y-K model; (e) Pixel intensity profiles for the selected black line in image (a); (f), (g), (h) The residuals corresponding to (b) (c) and (d), respectively.

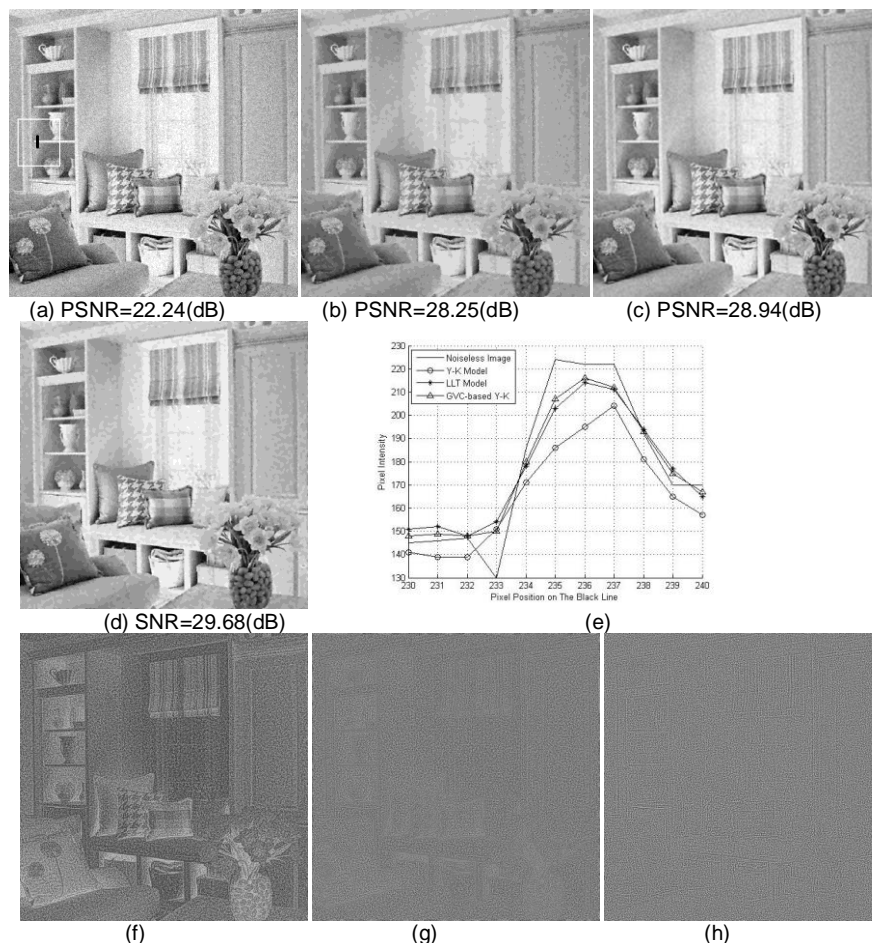


Fig.9. (a) Barbara image corrupted with Gaussian noise— $\mathcal{N}(0,20)$; (b) Y-K model; (c) LLT model; (d) GVC-based Y-K model; (e) Pixel intensity profiles for the selected black line in image (a); (f), (g), (h) The residuals corresponding to (b), (c) and (d), respectively.

5. Conclusion

In this paper, we proposed two novel diffusion models based on the GVC field. The first one is the GVC-based second order anisotropic diffusion and the second one is the GVC-based fourth order anisotropic diffusion model. Since the GVC field is very robust to noisy and it can be implemented in real time owing to its convolution mechanism, the proposed GVC-based anisotropic diffusions benefit much from the GVC models. These two proposed methods have many advantages over the existing models, such as better denoising

effects and better edge and texture preservation. Although the ability of denoising of the proposed GVC-based fourth order method is weak than the recent non-diffusion based LARK and BM3D, it is the best filter in the diffusion methods. We have conducted many experiments on different images with different noise levels. All of these qualitative and quantitative advantages of our proposed methods mean that both models can provide better image processing tools which enables noise removal, edge-preserving and staircase suppression.

Acknowledgement. This work was supported in part by the NSFC(60602050), the Key Project from the Tianjin Commission of Science and Technology(11JCZDJC15600, 10JCYBJC11000), and the Science and Technology Supported Key Project of Tianjin(11ZCKFGX00900, 10DZDZX00400)

References

1. Caselles V., Morel J. M., Sapiro G.: Tannenbaum A.: Introduction to the special issue on partial differential equations and Geometry-driven diffusion on image processing and analysis. *IEEE Trans. on Image Processing*, vol.7, no.3, 269-273. (1998)
2. Takeda H., Farsiu S., Milanfar P.: Kernel Regression for Image Processing and Reconstruction. *IEEE Trans. on Image Processing*, vol. 16, No. 2, 349-366. (2007)
3. Tomasi C., Manduchi R.: Bilateral filtering for gray and color images. *Proc. of the IEEE International Conference of Compute Vision*, 836–846. (1998)
4. Buades A., Coll B., Morel J.M.: A non-local algorithm for image denoising. *IEEE Computer Vision and Pattern Recognition*, vol. 2, 60-65. (2005)
5. Chatterjee P., Milanfar P.: Patch-Based Near-Optimal Image Denoising. *IEEE Trans. on Image Processing*, vol. 21, no. 4, 1635-1649. (2012)
6. Wang XY, Yang HY, Fu ZK: A New Wavelet-based image denoising using undecimated discrete wavelet transform and least squares support vector machine. *Expert System with Applications*, vol. 37, 7040-7049. (2010)
7. Fathi A., Naghsh -Nilchi AR.: An Efficient Image Denoising Method Based on a New Adaptive Wavelet Packet Thresholding Function. *IEEE Trans. on Image Processing*, vol. 21, no. 9, 3981-3990. (2012)
8. Dabov K., Foi A., Katkovnik V., Egiazarian K.: Image denoising by sparse 3D transform-domain collaborative filtering. *IEEE Trans. on Image Processing*, vol. 16, no. 8, 2080-2095. (2007)
9. Perona A. Malik J.: Scale-space and edge detection using anisotropic diffusion, *IEEE Trans. on Pattern Analysis and Machine Intelligence*, vol.12, no.7, 629 – 639. (1990)
10. You Y. L., Xu W. Tannenbaum A. Kaveh M.: Behavioral analysis of anisotropic diffusion in image processing, *IEEE Trans. on Image Processing*, vol.5, no.11, 1539-1553. (1996)
11. Scherzer O. Weickert J.: Relations between regularization and diffusion filtering, *Journal of Mathematical Image and Vision*, vol.12, no.1, 43-63. (2000)
12. Catte F., Lions P. L., Morel J.M., Coll T.: Image selective smoothing and edge detection by nonlinear diffusion, *SIAM Journal on Numerical Analysis*, vol.29, no.1, 182–193. (1992)

13. Alvarez L., Lions P. L., Morel J.M.: Image selective smoothing and edge detection by nonlinear diffusion. II, *SIAM Journal on Numerical Analysis*, vol.29, no.3. 845–846. (1992)
14. Osher S. J., Rudin L. I.: Feature-oriented image enhancement using shock filters, *SIAM Journal of Numerical Analysis*, vol.27, no.4, 919–940. (1990)
15. Rudin L. I., Osher S., Fatemi E.: Nonlinear total variation based noise removal algorithms, *Physical D*, vol.60, 259–268, (1992)
16. Alvarez L., Mazora L.: Signal and image restoration using shock filters and anisotropic diffusion, *SIAM Journal of Numerical Analysis*, vol.31, no.2, 590-605. (1994)
17. Gilboa G., Sochen N., Zeevi Y.: Forward-and-backward diffusion processes for adaptive image enhancement and denoising, *IEEE Trans. on Image Processing*, vol.11, no.7, 689-703. (2002)
18. Gilboa G., Sochen N., Zeevi Y. Y.: Image enhancement and denoising by complex diffusion processes, *IEEE Trans. on Pattern Analysis and Machine Intelligence*, vol.26, no.8, 1020-1036. (2004)
19. Black M. J., Sapiro G., Marimont D.H., Heeger D.: Robust anisotropic diffusion, *IEEE Trans. on Pattern Analysis and Machine Intelligence*, vol.7, no.3, 421 – 432. (1998)
20. Gilboa G., Zeevi Y.Y., Sochen N.: Texture preserving variational denoising using an adaptive fidelity term, *Proceedings of the VLISM, France*, 137–144. (2003)
21. Yu H., Chua C.S.: GVF-based anisotropic diffusion models, *IEEE Trans. on Image Processing*, vol.15, no.6, 1517–1524. (2006)
22. Xu C., Prince J. L.: Snakes, shapes, and gradient vector flow, *IEEE Trans. on Image Processing*, vol.7, no.3, 359-69. (1998)
23. Kass M., Witkin A., Terzopoulos D.: Snakes: active contour models, *International Journal of Computer Vision*, vol.1, no.4, 321-331. (1987)
24. Ghita O., Whelan P. F.: A new GVF-based image enhancement formulation for use in the presence of mixed noise, *Pattern Recognition*, vol.43, 2646-2658. (2010)
25. Sum A. K. W., Cheung P. Y. S.: Stabilized anisotropic diffusion, *IEEE International Conf. on Acoustics, Speech and Signal Processing*, vol.1, 709-712. (2007)
26. Wei G. W., Marimont D. H., Heeger D.: Generalized Perona-Malik Equation for Image Restoration, *IEEE Signal Processing Letters*, vol.6, no.7, 165–167. (1999)
27. You Y. L., Kaveh M., Fourth-order partial differential equations for noise removal, *IEEE Trans. on Image Processing*, vol.9, no.10, 1723–1730. (2000)
28. Lysaker M., Lundervold A., Tai X. C.: Noise removal using fourth-order partial differential equation with applications to medical magnetic resonance images in space and time, *IEEE Trans. on Image Processing*, vol.12, no.12, 1579-1590. (2003)
29. Wang Y., Jia Y.: External force for active contours: gradient vector convolution, *Pacific Rim International Conference on Artificial Intelligence*, 466-472. (2008)
30. Wang Z., Bovik A. C., Sheikh H.R.: Image quality assessment: from error visibility to structural similarity, *IEEE Trans. on Image Processing*, vol. 13, no.4, 1-14. (2004)
31. Krissian K., Westin C.F., Kikinis R., Vosburgh K.: Oriented speckle reducing anisotropic diffusion, *IEEE Trans. on Image Processing*, vol.16, no.5, 1412-1424. (2007)
32. Carmona R.A., Zhong S.: Adaptive smoothing respecting feature denoising, *IEEE Trans. on Image Processing*, vol.7, no.3, 353-358. (1998)
33. Lysaker M., Tai X. C.: Iterative image restoration combining total variation minimization and a second-order functional, *International Journal of Computer Vision*, vol.66, no.1, 5-18. (2006)

34. Blomgren P., Chan T.F., Mulet P.: Extensions to total variation denoising, Proceedings of SPIE, San Diego, vol. 3162, (1997)

Huaibin Wang is a professor and the vice dean of the School of Computer Science and Communication, Tianjin University of Technology, where he first joined by the end of 1988 and promoted to be a professor in 2000. He got his Bachelor degree at Jilin University in 1982 and completed his Master thesis in 1988 at Harbin Institute of Technology. During 1982-1986, he worked at China Agricultural Machinery Design and Research Institute. Prof. Wang has published more than one hundred papers in reputable journals and conference proceedings, covering the areas of computer vision, image processing and network security. Prof Wang has received many Chinese national prestigious academic awards, and has also been serving as an expert of information science panel, Tianjin committee of science and technology, China.

Yuanquan Wang is a professor of Computer Science and Communication, Tianjin University of Technology, where he was recruited as a Talent Professor in 2006, became yet a professor in 2012. He completed his Master and Ph.D. thesis at Nanjing University of Science and Technology (NUST) in 1998 and 2004, respectively, then joined the Beijing Institute of Technology (BIT) in 2004 as a postdoc. He won the most outstanding postgraduate award from NUST in 1998. During 1998-2001, he worked as a software engineer in industry. Prof. Wang has published dozens of papers in reputable journals and conference proceedings, covering the areas of Computer Vision, Image Processing and Medical Image Analysis, and his papers have gotten over 200 citations, including the citation by Nature Method journal.

Wenqi Ren received the B.S. degrees from the School of Information Engineering, Hebei University of Technology, in 2010. He is currently pursuing the Master degree in School of Computer Science and Communication Engineering, Tianjin University of Technology, working closely with Prof. Y. Wang and H. Wang. His current research interests is image processing focusing on PDEs and sparse representation.

Received: February 19, 2012; Accepted: December 06, 2012.

